Journal of Biomolecular Structure & Dynamics, ISSN 0739-1102
Volume 22, Issue Number 6, (2005)

Dynamics of the Native and the Ligand-bound Structures of Eosinophil Cationic Protein: Network of Hydrogen Bonds at the Catalytic Site

http://www.jbsdonline.com

B. S. Sanjeev
S. Vishveshwara*

Molecular Biophysics Unit
Indian Institute of Science
Bangalore 560 012
India

Abstract

Eosinophil Cationic Protein (ECP) is sequentially and structurally similar to ribonuclease A (RNase A). It belongs to the RNase A family of proteins and the RNA catalysis is essential to its biological function. In the present study, we have generated the dinucleotide-bound structures of ECP by superposing the dinucleotides-angiogenin structures to a large number of molecular dynamics (MD) generated ECP structures. The stability of the docked enzyme-ligand complexes was ascertained by extensive MD simulations. The modes of ligand binding are explored by the essential dynamics studies. The role of water molecules in the stability of the complex and in the catalysis is investigated. The active site residues form a complex network of connections with the ligand and with a water molecule. The catalytic mechanism of the RNA cleavage is examined on the basis of the active site geometry obtained by the simulations.

Introduction

Enzymes are known to catalyze reactions by lowering the activation barriers. A number of events should happen in a concerted manner to make the catalysis possible. Some of the important factors involved in the catalysis by an enzyme are, the mode of the ligand binding, the dynamics of the protein-ligand complex and the participation of water molecules. Experimental techniques such as crystallography, NMR, mutagenesis and kinetic studies can give insights into some of these aspects (1). We have been engaged in understanding the mode of ligand binding (2, 3), dynamics (4, 5), catalytic mechanism (6) and the influence of water molecules (7) on the structure and function of the Ribonuclease A (RNase A) family proteins from the perspective of computational biology.

The present focus is on Eosinophil Cationic Protein (ECP), which is a member of the RNase A family. ECP is present in eosinophil granules and exhibits diverse biological functions (8) such as anti-viral activity (9), neurotoxicity, helminthotoxicity, and anti-bacterial activity (10). ECP catalyses the cleavage of RNA and has high structural resemblance to RNase A (11). The structure of ECP in complex with 2',5'-ADP is available (12). However, the enzymes of RNase A family cleave the phospho-diester bond of the poly-nucleotides. Hence the binding of at least a dinucleotide to the protein should be investigated to gain insights into the catalytic mechanism. In addition, the substrate specificities differ from one member of the family of RNase A to other (13). Thus, the protein-ligand interactions can be classified into the 'catalytic region' and the 'substrate specificity region'. All the members of the RNase A family have the active site residues conserved and our focus is on this region of ECP-ligand interaction.

Our earlier work on angiogenin-ligand complexes (2) provided us the structures of the dinucleotides bound to angiogenin, which can possibly exist in the active-site of

Phone: 00 91 80 2293 2611
Fax: 00 91 80 2360 0535
Email: sv@mbu.iisc.ernet.in

the RNase A family of proteins. In the present study, we have docked the ligands onto ECP structures generated by the molecular dynamics simulations by superposing them onto the dinucleotide-angiogenin complexes. Furthermore, we have performed molecular dynamics simulations on these dinucleotide-bound ECP complexes. We have compared the dynamics of these systems to explore the stabilizing interactions, the essential modes of binding and especially the role of water. The present simulations on the ECP-dinucleotide complexes are carried out for longer time than in the earlier study on angiogenin ligand-complexes (2). This has aided in identifying the water molecules bound to the protein-ligand complexes for longer times (>500 ps). Consistent interactions have been observed among the three complexes of ECP, and have provided new insights into the catalysis of RNase A family of enzymes.

Materials and Methods

Generation of the Dinucleotide Docked Structures

Docking procedures in general carry out the conformational search of the ligands and the residues at the active site of the proteins. The conformation of the protein backbone and the side chain orientations in the regions other than the active site would normally be considered as rigid. In some cases, this poses a limitation on the success of the prediction of the ligand-docked structures. Such limitations, for instance, have been reported during the docking of the mononucleotide and the dinucleotide ligands into the active site of ECP (12). If the ligand bound structures of homologous proteins are available, the rigid geometry constraint on the protein can be overcome by superposing the ligand bound homologous protein structures onto a large number of protein snapshots obtained by the molecular dynamics simulations. In the present study, we have followed such a procedure to obtain the ligand bound structures of ECP. Three dinucleotides, namely CpG, CpA and UpA (Figure 1) were selected for docking on to ECP. The structures of the complexes were obtained by the following procedure. We had earlier generated the dinucleotide-docked structures of angiogenin, another member of the RNase A family, by molecular dynamics followed by simulated annealing method (14). In the present study, these dinucleotide structures were superposed on to a large number of ECP conformations generated by the MD simulations. The native structure of ECP (PDB code: 1DYT, A-chain) was simulated for a period of 5.4 ns and the snapshots were stored at every picosecond. Each of these 5400 snapshots was superposed on the ten dinucleotide-angiogenin complex structures using the program ALIGN (15). The complexes with steric clashes between the ligand and ECP were filtered. The structures of complexes, thus generated were further scanned for a set of functionally important protein-ligand interactions (2, 14) (also see Table I), and the filtered complexes were energy minimized. The distances between the protein and the ligand atoms in the structures finally selected for molecular dynamics simulations are given in Table I, and a cartoon representation of these docked structures, created with Raster3d (16), is shown in Figure 2. A few important protein-ligand interactions, also indicated in Table I, were constrained in the first 150 ps of the simulations.

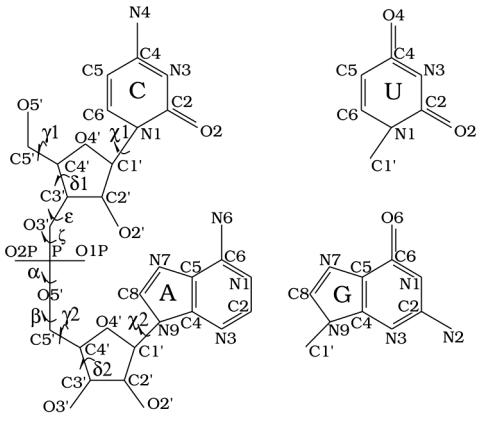

Figure 1: A schematic representation of the structures of the dinucleotide ligands, CpG, CpA and UpA considered for docking and simulations. The torsion angles defining the dinucleotide conformations are represented in the figure.

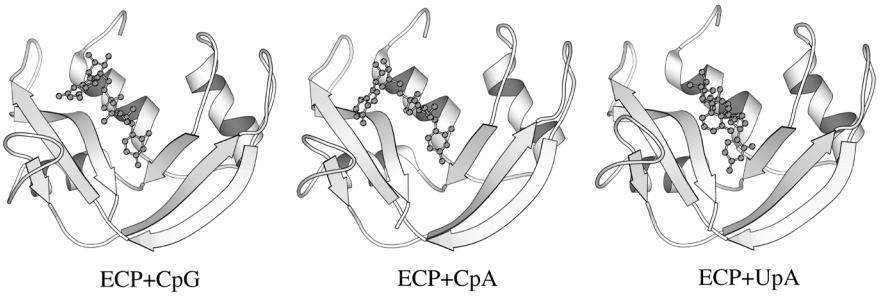

Figure 2: A cartoon representation of the structures of CpG, CpA and UpA bound complexes of ECP obtained by the docking procedure and used as the starting structures for MD simulations.

Table I

Distances between some of the important pairs of atom of the protein and the ligands of the dinucleotide bound ECP complexes in minimized structures. The set of interactions, which were used (neglected) for screening the ligand-bound structures are marked 3 (×).

Protein atom – Ligand atom[a]	Distance[b]		
	ECP+CpG	ECP+CpA	ECP+UpA
Gln14(NE2) - RX3(O2P)	2.78(N) ×	2.87(N) ×	6.77(N) ×
His15(NE2) - RX3(O1P)	3.66(N) 4	3.72(N) 4	4.65(N) 4
His15(NE2) - RY5(O2)	3.63(C) 4	3.62(C) ×	3.19(C) 4
Lys38(NZ) - RY5(O2)	3.84(C) 4	3.38(C) 4	2.87(C) 4
Lys38(NZ) - RY5(O2)	2.83(C) 4	2.70(C) 4	5.59(C) 4
Thr42(N) - RY5(N3)	4.05(C) ×	3.65(C) 4	4.83(C) ×
Thr42(OG1) - RY5(N3)	2.91(C) ×	3.93(C) 4	3.08(C) 4
Thr42(OG1) - RY5(N4/O4)	2.92(C) 4	3.06(C) 4	4.60(C) ×
His128(ND1)- RX3(O1P)	2.96(N) 4	3.05(N) 4	2.80(N) 4
His128(ND1)- RX3(O5)	2.87(C) ×	2.83(C) 4	2.93(C) ×
Leu129(N) - RX3(O1P)	3.01(C) 4	3.17(C) 4	3.90(C) 4

[a]X is pyrimidine and Y is purine. [b]C(N) indicates that the distance (in) between the pair of atoms is constrained(not-constrained) in the initial 150 ps of simulation. If the angle was also constrained, it is highlighted in bold (C).

Simulation Protocol

Molecular Dynamics (MD) simulations were performed using AMBER7 package (17) with the parm98 parameters (18). Each simulation comprised 500 ps equilibration run followed by 3 ns of simulation in TIP3P water (19). The solvation box was 8 Å from the farthest atom along any axis. This resulted in about 5300 water molecules in each system. Particle Mesh Ewald summation (20) was used for the long-range electrostatics and Van der Waals cut-off was 10 Å. The pressure and the temperature relaxation were set to 0.5 ps^{-1}. The simulations were performed under NPT conditions. The first 500 ps of simulation was the equilibration phase and the rest was used for analysis. The coordinates were stored after every picosecond of the simulation. His15, which is uncharged, has proton at ND1, while His128 is positively charged (21). The temperature of the system was raised from 0 K to 100 K during the first 10 ps, to 200 K in the next 10 ps and finally to 300 K by 30 ps. The first 150 ps of simulation was constrained as listed in Table I. The constraints were removed completely from 150 ps onwards.

Essential Dynamics Analysis

The essential dynamics (ED) analysis is a robust method to identify "essential" subspace from the protein dynamics (22). A detailed account of this application has been given elsewhere (5) and is presented briefly in what follows. For each simulation, the 3000 snapshots obtained from the MD trajectory during the production run were superimposed with respect to the average MD structure using all C^{α} atoms. The covariance matrix was then constructed. All atoms of the protein were considered for the construction of all-atom covariance matrix and only the C^{α} atoms were used for the construction of C^{α}-covariance matrix. MATLAB6 was used to obtain the eigenvalues and the eigenvectors. The eigenvectors represent the directions of motions of the atoms and the eigenvalues represent the total mean square fluctuation of the system along the corresponding eigenvectors.

The dynamic properties of any two similar proteins *a* and *b*, with eigenvectors $\{\eta^a\}$ and $\{\eta^b\}$ respectively, can be compared using the root-mean-square inner product (RMSIP) between the corresponding top ten eigenvectors. RMSIP is defined (23) as:

$$RMSIP = \sqrt{\frac{1}{10}\sum_{i=1}^{10}\sum_{j=1}^{10}(\eta_i^a.\eta_j^b)^2}$$

The RMSIP gives the similarity between the two sets of the "essential modes", with zero indicating no similarity and unity for complete similarity.

Hydrogen Bond Analysis

A standard distance criterion of 3.5 Å or less between the donor and the acceptor atoms, and the deviation from linearity of donor-hydrogen-acceptor angle within 60° were used to define a hydrogen bond. Hydrogen bonds between the polar atoms (nitrogen and oxygen) of the protein were divided into two types: Mainchain Hydrogen Bond (McHB), the hydrogen bond in which both the donor and the acceptor atoms were from the mainchain, and Side chain Hydrogen bond (ScHB), the hydrogen bond in which at least one atom was from the side chain(s). In the context of protein-ligand complex, the nucleotides were treated as non-mainchain atoms and therefore the protein-ligand interactions were placed under ScHBs.

Hydration Analysis

The hydration analysis based on an extensive MD simulation employed in the present study was described in an earlier article (7). Briefly, the hydration analysis was carried out on the 3000 snapshots of the coordinates obtained from each of the simulations. Residence time of a polar atom with a water molecule was defined as the number of coordinate sets (stored at every 1 ps) in which the donor-acceptor pairs come within a distance of 3.2 Å. Every water molecule was labeled, and the residence times of all the polar atoms were determined. We identified all the protein-water and the water-water interactions with residence times greater than 500 ps, *i.e.*, the interaction being present continuously in more than 500 snapshots. The maximum residence time (MRT) of an atom is the maximum of its residence times with the water molecules. A donor-acceptor distance of 3.2 Å and a deviation of the donor-hydrogen-acceptor away from linearity within 60° characterize an acceptable hydrogen bond between a protein atom and a water molecule. We have shown that a spatial-temporal (S-T) criterion (7), which is the distance constraint of 3.0 Å obeyed by the interaction between a tagged water molecule and a protein polar atom with residence times higher than 500 ps, can accurately (>97%) capture the angle distribution. We have relaxed the distance criterion to 3.2 Å as was suggested by the radial distribution of the water molecules around the polar atoms, but verified that 3.2 Å also is almost as good in satisfying the angle criterion. The argument for the S-T criterion was that a water molecule staying proximal to a protein polar atom for a very long period arises due a good hydrogen bond between them. Clustering algorithm was used to identify the water networks. When two protein atoms have residence times higher than 500 ps involving the same water molecules then it was considered as a bridging water molecule. Any cluster that had more than two protein atoms with MRT higher than 500 ps and bridged by a water molecule(s) was considered as a water network.

Results and Discussion

Molecular Dynamics and the Essential Modes

The dinucleotide-bound ECP complexes, generated as explained in the ***Materials and Methods*** section, were subjected to 3.5 ns molecular dynamics (MD) simulations. The Root-Mean Square Deviations (RMSDs) of ECP and those of the ligands (LigRMSD) from the simulations of ECP-bound ligand complexes are shown in Figure 3. The residue-wise RMSDs (RRMSDs) of the ECP complexes are also shown. The RMSDs along the trajectories in all the three complexes were less than 0.9 Å from the MD average structures. The RMSDs with respect to the starting structure was about 1-1.5 Å in CpG and UpA complexes. However, it increased to about 2 Å in the CpA complex after 1.5 ns. An examination of the protein structures revealed that there was a widening of the gap in the region connecting the N-

terminus with the loop preceding the C-terminal strand in the CpA complex. This is also reflected in the RRMSDs of these two regions. The RRMSD in all the three complexes are relatively high for the regions corresponding to the first helix, the loop consisting of residues Ile60-Asn70 (known as the second base binding region) and the loop preceding the C-terminal strand. The average MD (<MD>) conformation of the ligands have deviated from the starting structure with LigRMSD of about 1 Å from the beginning of the simulations in CpG and UpA complexes. The deviation of <MD> conformation increases from the starting structure of CpA complex after 1.5 ns. This correlates with the RMSD change in the protein.

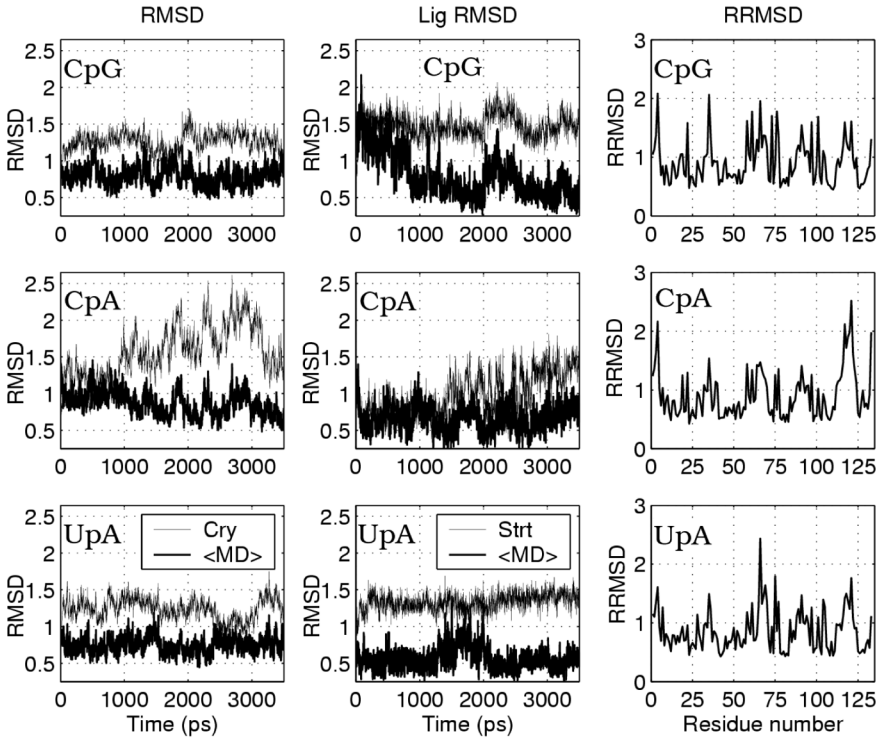

Figure 3: The MD trajectories of the ligand-bound complexes of ECP. The root mean square deviations RMSD (Å), LigRMSD (Å) and RRMSD (Å) correspond to the protein, the ligand and the residue-wise deviations in the protein respectively.

The important dynamical behavior of a protein can be captured by the top modes of the essential dynamics. The flexible loop regions and the terminal regions contribute significantly to these top modes in all the cases. The contribution to the top three modes comes mainly from the loop regions Ile60-Asn70 and Ala110-Val124 in the native protein. The N-terminal helix and the loop regions Arg28-Trp35 and Leu85-Asn95 along with the loop preceding the C-terminal strand Ala110-Val124 contribute significantly in the ligand bound structures.

A quantitative comparison of the essential dynamics of any two related systems can be made by the parameter RMSIP (see materials and methods section). The RMSIP values consisting of the top ten modes amongst the four systems are presented in Table II. The RMSIPs computed from the C^{α} atoms as also from all the atoms are given in the upper and the lower triangles respectively. As expected, the correlations in general are better at the backbone level than at the level of all-atoms. It is interesting to note that the dynamics of all the three ligand-bound structures are more similar to each other (C^{α}-RMSIPs around 0.8) than to the native structure (C^{α}-RMSIPs around 0.54).

Table II

RMSIPs of the ligand-bound and the native ECP for the top 10 modes. C^{α} RMSIP is shown in bold font and all-atom RMSIPs in normal font.

	ECP + CpG	ECP + CpA	ECP + UpA	ECP
ECP + CpG	-	**0.82**	**0.80**	**0.53**
ECP + CpA	0.66	-	**0.80**	**0.57**
ECP + UpA	0.63	0.67	-	**0.54**
ECP	0.44	0.42	0.41	-

Ligand Conformation

The conformations of the dinucleotides CpG, CpA and UpA are represented by a set of dihedral angles given in Figure 1. The average values of these parameters obtained during the simulations are presented in Table III. The conformational properties of RNA are available in the literature (23). A comparison of the conformational parameters given in Table III with the conformational parameters of RNA showed that the set of values fall into one or two low frequency conformers. It is interesting to note that the dinucleotide in the active site scans only a limited set of RNA conformers during the dynamics, although the dinucleotide is more flexible than a polymer chain of the RNA molecule. However, significant variations in the values around the average were also seen. Furthermore, the values of (ζ,α) is close to (g,g) conformation around the phosphodiester bonds, which is known to be preferred due to anomeric effect (25, 26). The β value is close to trans conformation (which was identified as the high frequency conformation) in CpG and UpA, whereas it is close to the low frequency value in CpA (27). Similar values are taken by χ_1 in all the three simulations and in contrast, the χ_2 values are different in the three simulations. This reflects the mobility of the purine base that is on the open end of the active site unlike the pyrimidine base, which is located at the narrow end of the active site pocket. It is consistent with the experimental observations, which show that the pyrimidine base binding residues are well characterized than the purine base binding residues of RNase A family proteins (28).

Table III

Average values of the backbone torsion angles of the dinucleotides bound to ECP from the simulations.

	CpG (°)	CpA (°)	UpA (°)
γ_1	27.2 – 51.8	71.1 – 41.2	-166.8 – 15.3
δ_1	110.4 – 23.4	87.4 – 12.2	79.1 – 9.2
ε	-142.3 – 14.0	-158.6 – 21.9	-165.8 – 19.1
ζ	74.5 – 10.5	69.8 – 25.8	65.3 – 10.2
α	74.6 – 13.7	90.2 – 28.0	64.9 – 11.2
β	173.3 – 16.3	89.6 – 29.6	176.9 – 16.5
γ_2	-166.1 – 10.3	178.2 – 9.3	-173.2 – 9.1
δ_2	103.3 – 29.1	142.5 – 20.7	128.8 – 28.9
χ_1	-129.7 – 15.9	-129.4 – 14.4	-99.3 – 18.9
χ_2	-150.3 – 19.9	-95.6 – 20.9	-41.9 – 18.7

Dynamically significant hydrogen bonds

Intra-protein ScHB: The trajectories of the hydrogen bonds involving the side chain atoms are monitored during the simulations. It is to be noted that a few of these hydrogen bonds (Table IV) are stable (>96%) during almost the entire simulation period in all the docked systems. Except Asn51(ND2)-Arg73(O), all the other interactions were highly stable in unbound enzyme as well. Several of these interactions include the residues which are important, either from the function (Gln14 and Lys38) or from the folding (Tyr98) point of view and these three residues are also conserved in the RNase A family of enzymes. It is interesting to see that both the mainchain 'N' and 'O' atoms of the catalytically important residue Lys38 are strongly stabilized by interaction with the side chain atoms of other residues. Further, the mainchain oxygen of Arg73 is strongly held (>97%) by Asn57(ND2) in all the ligand bound structures. It is an indication that the loop region Ile60-Asn70, which is presumably involved in the interaction with the purine base, is rigid in the ligand bound structures. Apart from these completely stable interactions, there are several partially stable interactions involving the N-terminal region and the residues in the loop preceding the C-terminal strand (Table IV). The interactions between the atoms of Arg117 and Asp115 are highly stable in all the simulations with the exception of the CpA complex. The CpA complex also exhibits not so stable interactions between the N-termi-

nal residues and the side chains of Arg117 and Asp118, which are more stable in ECP bound to CpG, UpA and the native ECP. This feature is correlated with higher RMSD (after 1.5 ns) and RRMSD values corresponding to the region Asn113-Pro120 in the CpA bound complex (Figure 2), in comparison with the simulations on the other systems. This results in the expansion of the pore in this important ligand-binding region.

Table IV

Percentage occurrence of some of the important intra-protein H-Bonds seen in the three complexes and in native system during the simulation. The H-bonds in normal font are those that bridge N-C termini. A H-bond in this region is reported if it has at least 25% occurrence in any one of the three ligand-bound systems. The H-bonds highlighted in **bold** are those that occur for at least 96% of the time in all the three ligand-bound systems.

Interaction					ECP+CpG	ECP+CpA	ECP+UpA	ECP
THR	6 OG1	-	ASP	118 OD1	32.2	6.1	16.7	18.7
THR	6 OG1	-	ASP	118 OD2	60.7	18.1	48.8	53.9
ARG	7 NH1	-	ASP	112 OD1	20.7	32.2	27.3	17.1
ARG	7 NH1	-	ASP	112 OD2	49.7	33.9	29.8	53.7
ARG	7 NH2	-	ASP	112 OD1	28.6	39.6	13.1	21.0
ARG	7 NH2	-	ASP	112 OD2	57.2	44.1	3.3	65.1
ARG	7 NH2	-	ASN	113 O	13.9	25.4	0.0	12.3
GLN	9 NE2	-	ASP	118 OD1	28.7	6.0	21.6	18.6
ARG	117 NH1	-	PRO	3 O	26.5	11.3	25.5	42.1
ARG	117 N	-	ASP	115 OD1	99.0	32.9	98.7	99.1
ARG	117 NE	-	ASP	115 OD1	99.1	47.7	99.2	94.7
ARG	117 NH2	-	ASP	115 OD2	98.9	68.7	99.1	94.2
ARG	**1 NH1**	**-**	**PHE**	**5 O**	**97.4**	**99.7**	**96.4**	**98.9**
LYS	**38 N**	**-**	**ASN**	**31 OD1**	**99.9**	**99.8**	**99.6**	**100.0**
ASN	**41 ND2**	**-**	**GLN**	**14 O**	**99.9**	**99.9**	**99.9**	**97.7**
ASN	**57 ND2**	**-**	**ARG**	**73 O**	**97.1**	**99.2**	**98.6**	**78.6**
ARG	**97 N**	**-**	**ASN**	**87 OD1**	**99.3**	**99.7**	**98.1**	**99.5**
TYR	**98 N**	**-**	**THR**	**24 OG1**	**99.3**	**99.5**	**98.1**	**99.0**
TYR	**98 OH**	**-**	**LYS**	**38 O**	**100.0**	**100.0**	**100.0**	**100.0**

Protein-ligand and Intra-ligand Interactions: The protein-ligand and the intra-ligand interactions, which are significant, have been presented in Table V. Although these interactions are not as stable as the intra-protein interactions discussed above, they are significant from the ligand binding and the catalysis points of view. It can be seen from Table V that many of the crucial interactions between the protein and the ligands are present for a significant amount of time. At the 5′-end, the pyrimidine base (cytosine/uracil) is strongly bound to the Thr42 residue. Both the backbone polar atoms and the OG1 of the side chain of Thr42 take part in the interactions with the pyrimidine base. This is consistent with the observations from several ligand-bound structures (28, 21) and earlier simulation results on RNase A (3). The interaction with the purine base at the 3′-end on the other hand, is not as stable as that of the pyrimidine base. In fact, the only stabilizing interaction of the purine base with Asn70 is seen in the case of the CpA complex. This is also consistent with the experimental observation that the purine-base binding region is not well defined (29). Furthermore, it correlates well with the fact that the purine base adopts different conformations in the three simulations whereas the pyrimidine base adopts very similar conformation in the three simulations. Although some differences are seen in the base binding regions of different ligands, a remarkable consistency is seen in the intra-ligand and protein-ligand interactions of the catalytic region in the three simulations. The atoms/residues involved in these interactions are O2′ (of the ribose on the 5’-end), O1P, O5′ (on the 3’-end), His15, His128, and Leu129. It is interesting to note that among these atoms, O2′ and O1P are involved in multiple hydrogen bonds. The interactions of O2′ with O1P and Lys38(NZ) are considerably stable, whereas its interactions with O3′ and His15 are intermittent. The relevance of all these interactions for catalysis is discussed in a later section.

Table V

The percentage occurrence of the protein-ligand and the intra-ligand interactions (H-Bonds) seen in the three complexes during the simulation.

Protein-ligand interaction[a]						CpG[b] (%)	CpA (%)	UpA (%)
LYS	38	NZ	-	RX5	O2	40.9 (A)	61.4 (A)	58.9 (P)
LYS	38	NZ	-	RX5	O3	-	-	35.0 (A)
LYS	38	NZ	-	RY3	O1P	-	22.4 (A)	6.1 (A)
GLN	40	NE2	-	RX5	O4	-	6.1 (A)	28.3 (A)
GLN	40	NE2	-	RX5	O5	-	2.8 (A)	35.9 (A)
THR	42	OG1	-	RX5	N3	56.5 (P)	70.7 (A)	-
THR	42	OG1	-	RX5	O2	15.6 (A)	38.0 (A)	5.7 (P)
ASN	70	ND2	-	RY3	N1	-	75.6 (A)	-
HIS	128	ND1	-	RY3	O1P	60.7 (A)	52.9 (A)	74.3 (P)
HIS	128	ND1	-	RY3	O5	21.9 (P)	57.4 (P)	3.5 (P)
LEU	129	N	-	RY3	O1P	0.7 (P)	31.3 (P)	0.8 (A)
THR	132	OG1	-	RX5	O4	-	-	60.0 (A)
RX5		O2	-	HIS	15 NE2	2.1 (A)	5.5 (A)	1.2 (A)
RX5		N3	-	THR	42 OG1	-	-	50.4 (P)
RX5		N4	-	THR	42 OG1	49.8 (P)	35.6 (P)	-
RX5		O5	-	ASP	130 O	55.9 (A)	-	-
RX5		O5	-	ASP	130 OD1	20.8 (A)	-	-
RX5		N4	-	THR	132 OG1	81.3 (A)	35.5 (A)	-
RY3		N6	-	ASN	70 OD1	-	78.3 (A)	-
Intra-ligand								
RX5		O2	-	RX5	O3	20.8 (A)	9.3 (A)	4.0 (A)
RX5		O2	-	RY3	O1P	48.2 (A)	53.8 (A)	65.0 (P)
RX5		O2	-	RY3	O2P	0.1 (P)	6.2 (P)	-

[a]X is pyrimidine and Y is purine. [b]The presence(absence) of these interactions in the starting structures chosen for simulations is indicated in brackets with P(A).

Hydration Studies

The hydration analysis has been carried out by explicitly tagging all the water molecules in the simulations and then identifying all interactions of the water molecules with the polar atoms of the protein-ligand complexes as described in the ***Materials and Methods*** section. All protein-water and the water-water interactions with residence times greater than 500 ps were identified. The term Maximum Residence Time (MRT) of an atom was defined as the maximum of the residence times of all the water molecules interacting with that particular protein atom or a water molecule. Our earlier work on RNase A and angiogenin (7) showed that in general the protein atoms with high MRT are a part of a protein-water network. In other words, a water molecule could hydrogen bond with a specific protein atom for an extended period more easily when the water molecule is involved in multiple interactions.

In the present study, we have identified such water networks in all the three complexes, and in the native ECP and the results are presented in Table VI. It is impressive to observe that the water networks and the hydration sites (sites with high MRT) in all the four simulations are remarkably similar. This emphasizes the inherent nature of proteins to retain water molecules at specific sites and to form network of interactions including water molecules. It is also interesting to note that the networks involve the loop regions and the active site regions of ECP (Table VI). The networks A1-A3 describe the interactions between the N-terminal region and the loop preceding the C-terminal strand. Several intra-protein hydrogen bonds were also noticed in this region (Table IV). The loop region, which is involved in binding of the purine base is stabilized by the networks (C1-C3) consisting of the residues Asn57, Gln58 and Arg73. Although these residues are polar, involvement of the backbone atoms are seen in the protein-water networks as well as in the direct hydrogen bonding, conferring additional stability to the loop. Similar stabilization of two other loops on the other parts of the protein (networks D1-D4) is also seen in all the four simulations. The binding of ligands seems to have made a significant change in the com-

Table VI

The protein-water networks[a] in the native and the ligand-bound ECP complexes identified through simulations.

Network	ECP + CpG		ECP + CpA		ECP + UpA		ECP	
A1	Ala 8(N)	[853]	Ala 8(N)	[1378]	Ala 8(N)	[730]	Ala 8(N)	[726]
	Asn113(O)	[832]	Asn113(O)	[874]			Asn113(O)	[1696]
	Asp115(N)	[824]	Asp115(N)	[705]	Asp115(N)	[770]	Asp115(N)	[835]
	Asp118(OD2)	[1712]	Asp118(OD2)	[587]	Asp118(OD2)	[1432]	Asp118(OD2)	[2422]
	Asp118(OD1)	[557]					Asp118(OD1)	[774]
	Ser119(O)	[1669]	Asp118(OD1)	[578]	Ser119(O)	[1497]	Ser119(O)	[4452]
	Tyr122(O)	[1615]	Ser119(O)	[1593]	Tyr122(O)	[1441]	Tyr122(O)	[4106]
			Tyr122(O)	[1380]				
A2	Arg 7(N)	[585]			Arg 7(N)	[1007]		
	Asp115(OD2)	[697]			Asp115(OD2)	[1344]		
A3					Arg 7(O)	[596]		
					Val127(O)	[563]		
B1	His 15(NE2)	[1371]	His 15(NE2)	[2116]	His 15(NE2)	[2689]		
					His128(ND1)	[1106]		
	Leu129(N)	[1448]	Leu129(N)	[1756]	Leu129(N)	[2650]		
	RG3 (O1P)	[1625]	RA3 (O1P)	[2285]	RA3 (O1P)	[2950]		
B2	Thr 42(N)	[500]						
	RC5 (O2)	[618]						
B3	Thr 42(OG1)	[682]			Thr 42(OG1)	[625]		
	Thr132(OG1)	[574]			Thr132(OG1)	[605]		
B4					Arg114(NH1)	[552]		
					Asp115(O)	[577]		
					Asp118(O)	[549]		
B5			Asp130(OD1)	[1108]				
			RA3 (N7)	[815]				
			RA3 (N6)	[797]				
B6					Asp130(O)	[642]		
					RA3 (N3)	[742]		
					RA3 (O4)	[632]		
C1	Asn 50(ND2)	[590]	Asn 50(ND2)	[617]				
			Asn 50(OD1)	[549]	Asn 50(OD1)	[519]	Asn 50(OD1)	[1485]
			Asn 53(OD1)	[514]				
	Arg 75(N)	[962]	Arg 75(N)	[1608]	Arg 75(N)	[588]	Arg 75(N)	[1066]
					Tyr107(OH)	[598]	Tyr107(OH)	[1456]
C2			Asn 57(ND2)	[543]				
	Gln 58(O)	[2922]	Gln 58(O)	[2954]			Gln 58(O)	[2623]
	Arg 73(N)	[2865]	Arg 73(N)	[2936]			Arg 73(N)	[2228]
C3	Asn 70(O)	[521]					Asn 70(O)	[959]
	Cys111(N)	[507]					Cys111(N)	[666]
							His 72(NE2)	[1191]
							Cys111(O)	[585]
D1	Arg 22(NE)	[509]	Arg 22(NE)	[522]			Arg 22(NE)	[607]
					Arg 22(NH1)	[598]		
	Cys 23(N)	[519]	Cys 23(N)	[789]				
	Thr 24(N)	[1488]	Thr 24(N)	[2647]	Thr 24(N)	[1959]	Thr 24(N)	[2436]
	Thr 24(OG1)	[982]	Thr 24(OG1)	[1565]	Thr 24(OG1)	[739]	Thr 24(OG1)	[910]
	Tyr 98(O)	[1303]	Tyr 98(O)	[2176]	Tyr 98(O)	[2208]	Tyr 98(O)	[3160]
	Asp100(OD1)	[1345]	Asp100(OD1)	[2976]	Asp100(OD1)	[2442]	Asp100(OD1)	[4364]
	Asp100(OD2)	[1184]						
D2	Thr 24(O)	[1716]	Thr 24(O)	[1163]			Thr 24(O)	[1079]
	Arg 28(NE)	[786]	Arg 28(NE)	[566]	Arg 28(NE)	[574]		
	Asn 31(ND2)	[1181]	Asn 31(ND2)	[1826]	Asn 31(ND2)	[1500]	Asn 31(ND2)	[1481]
	Ile 93(O)	[1226]	Ile 93(O)	[1804]	Ile 93(O)	[1599]	Ile 93(O)	[1682]
					Ser 94(O)	[533]		
	Cys 96(O)	[1888]	Cys 96(O)	[1256]	Cys 96(O)	[712]	Cys 96(O)	[1083]
D3	Cys 37(N)	[2085]	Cys 37(N)	[2701]			Cys 37(N)	[2698]
	Ala 90(O)	[2287]	Pro 88(O)	[926]			Ala 90(O)	[3304]
	Gln 91(O)	[1742]	Ala 90(O)	[2689]			Gln 91(O)	[3349]
			Gln 91(O)	[2568]				
D4					Gln 91(N)	[1809]		
					Asn 92(N)	[1588]		

[a]The networks given here are connected through water molecule(s). the numbers with in the square brackets ([]) indicate the maximum residence time of the corresponding atom.

position of the network (B1-B6), involving the active-site residues. In all the three ligand-bound complexes, the phosphate oxygen (O1P) of the ligands is involved in the water network with Leu129(N) and His15(NE2) (additionally, His128(ND1) is also involved in the UpA complex). These water-mediated interactions are further reinforced by the direct involvement of O1P in several intra-ligand and protein-ligand hydrogen bond interactions (Table V). In contrast, His15(ND1) in the native ECP is involved in a strong water network with another ligand binding residue Thr42(O & N). In this context, it should be noted that the participation of water molecules in the active site is commonly found in several proteins (30).

The stability of the water network at the active site, which involves the atoms of the protein and the ligand (His15(NE2), Leu129(N) and O1P) can be seen from the trajectories presented in Figure 4. A remarkable feature that can be observed is that a single water molecule connects all the crucial atoms in the CpG and the CpA complexes. The connecting water molecule is exchanged only once in each of the simulations, reiterating the stability of these networks. Furthermore, the corresponding network is even more stable without any exchange of water molecules during the simulation and includes the participation of the fourth atom (His128(ND1)) in the UpA complex. This is indeed an interesting case from the point of view of catalysis, since the network connects two histidine residues involved in the proton transfer process (31, 32, 33).

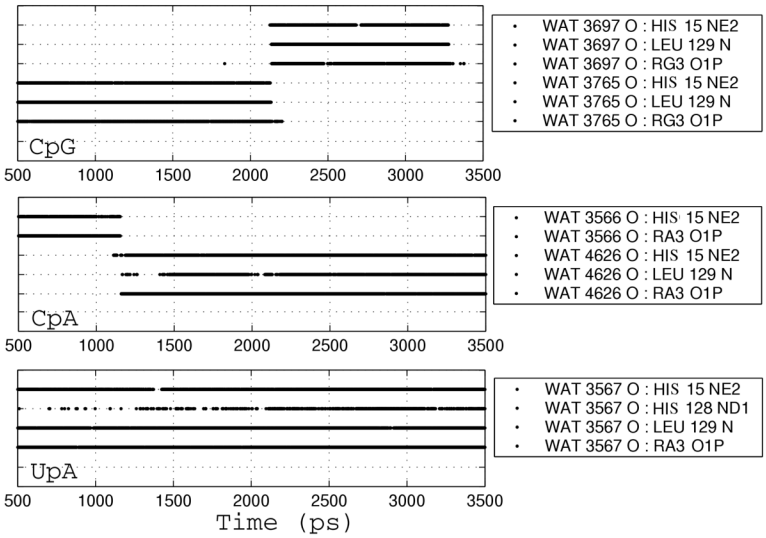

Figure 4: The trajectories of water networks (B1 in Table VI) involving the active-site region. The water numbers refer to the specific tagged water molecules in the simulations.

The Ligand Binding Modes

A significant amount of experimental information on the binding of the ligands to RNase A and to the other members of the RNase A superfamily is available (21). As mentioned earlier, the proteins of RNase A gene superfamily perform a variety of cellular functions. However, all of them perform the essential role of hydrolyzing the RNA molecule, although there is a wide variation in their substrate specificities. For example, both RNase A and angiogenin act on natural tRNA, synthetic polynucleotides, as well as on small molecules such as dinucleotides, with angiogenin exhibiting a weaker RNase activity on its substrates (34). The proteins of the eosinophil granules, ECP and EDN prefer to act on the RNA molecule with pyrimidine bases, with the highest activity being displayed towards poly (U) (35, 36). Both these proteins are less active towards small substrates such as 2′-3′ phosphates and the dinucleotide phosphates (37).

In the case of RNase A, it is known to have several binding subsites identified as p0, p1, p2, R1, R2 B1, B2, *et cetera*, with the phosphate groups, the ribose, and the bases occupying respectively the ‘p’, ‘R’, and the ‘B’ sites (38, 39). The phosphate moiety of the phospho-diester bond hydrolyzed by the enzyme is known to

bind to the p1 site and interact with the residues His12, Lys41 and His119. The B1-base binding site in RNase A contains the residue Thr45 and has been the region of the active site, which is very well characterized. In contrast, the interactions, conformation and/or orientation of the ribose and the phosphate of the R1 and p1 subsites show considerable variations even in the case of RNase A (40). The orientation of the phosphate in the p1 subsite is dependent on whether it is linked to the ribose through 2′- or 3′- ester linkage.

The above mentioned multiple subsites identified in RNase A are likely to be present in all the other members of the RNase A superfamily as well. The p1 subsite has been recognized as the 'catalytic region' and the rest of the subsites as the 'binding region' of the active site of these enzymes (38). The substrate specificities may arise due to the interactions at the 'binding region'. The binding of the phosphate moiety of the substrates, susceptible for catalysis should specifically take place at the catalytic region. In the case of ECP, this site contains the residues His15, Lys38, and His128, which are required (10) for the hydrolysis of the phospho-diester bond. However, the atomic details of the interaction of these residues with the substrate-like phosphate group are sensitive to the type of ribose-phosphate linkage. The specific details of the interactions at the atomic level have been elucidated for RNase A (3, 40) and angiogenin (2, 41). In our present study we have focused on this catalytic region of ECP. Although the dinucleotides are not good substrates for ECP, they contain the crucial phospho-diester bond, which is cleaved by all the members of the RNase A superfamily. They also contain the bases, which bind to the binding regions of the B1 and B2 subsites. The dinucleotide ligands are thus chosen in our present study as the model compounds for the real substrates.

Experimentally, the crystal structure of 2′-5′ diphosphate (ADP) bound ECP is available (12). So far, this is the only available crystal structure of the ligand bound to ECP. This has given us a glimpse of the mode of ligand binding to ECP, with the crucial residues such as Glu14, His15, Lys38, and His128 interacting with the ligand. The molecule binds at the p1 and B2 subsites. However, the phosphate group is attached to the 2′- oxygen of the ribose in this ligand, thus making the 2′-OH group inaccessible for catalytically important interaction. Furthermore, the absence of the pyrimidine base to bind at the B1 site and the freely rotating 2′-phosphate group can lead to non-specific interactions, although the phosphate group is within the catalytic region. In our present study, the pyrimidine bases of the dinucleotides have good interactions with Thr42, consistent with what was observed in the case of RNase A and angiogenin. In addition, consistent interactions with crucial residues of the catalytic regions are also seen in all the three dinucleotide docked structures that are stable during the simulations. Thus, we believe that the mode of ligand binding to ECP, which we have characterized in the present work, is a good representation of the interactions at the catalytic region and can be considered seriously to understand the catalytic mechanism of ECP and the other members of the RNase A family.

The Catalytic Mechanism

Enzymes are known to catalyze the reactions by reducing the activation barriers (38, 42, 43). However, gaining insights into the changes that take place at the atomic level during catalysis is difficult since it is a cumulative effect of multiple parameters as well as a dynamical process. Based on experimental evidences, several mechanisms have been proposed for the catalytic action of RNase A (31, 38, 42, 44). In general, it is considered as an acid-base catalysis, which involves two histidine residues of the enzyme, supported by a lysine. The rate-limiting step before the cleavage of the phosphodiester bond is considered to be the formation of the cyclic phosphate intermediate. The postulated mechanisms include the two-proton shift and simultaneous proton transfer (31), the short-strong hydrogen bond (32), and the intra-ligand proton transfer (33) as depicted schematically in Figure

5. Molecular dynamics studies (45-46) and further optimization of the coordinate snapshots from the molecular dynamics simulations (47) have also yielded some interesting information on the possible mechanism. Our present analysis of the three dinucleotide-bound ECP simulations has revealed an extensive hydrogen bonded network involving the protein-ligand-water molecule. Furthermore, this network is dynamically stable as discussed in an earlier section. A schematic representation of the crucial hydrogen bonds involving the atoms of the protein-ligand-water molecules is depicted in Figure 6. The resultant active-site geometry indicates that it can accommodate many of the previously proposed mechanisms. The participation of a water molecule facilitates the inter-linking of several crucial atoms by providing a scope for a relay of protons among them. Hence, we propose that the active-site geometry is like a 'melting pot' involving several protein-ligand-water interactions during the catalysis of RNA by RNase-A family proteins.

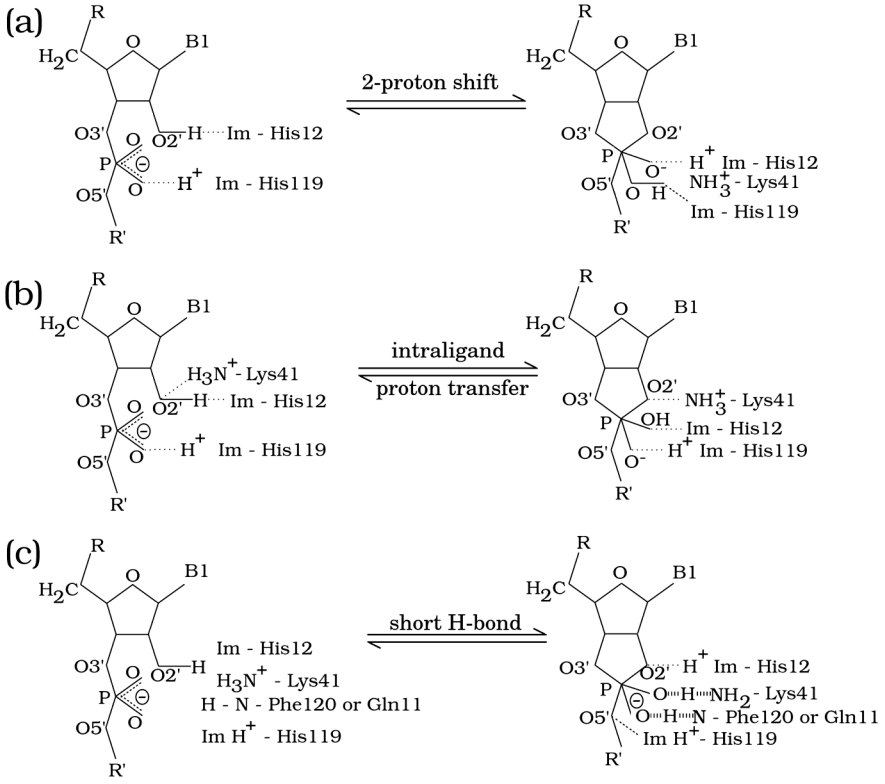

Figure 5: The three of the mechanisms for transphosphorelation of RNA by RNase A proposed by (**a**) Breslow *et al*., (**b**) Lim and Tole and, (**c**) Gerlt and Gassman. The residues Gln14, His15, Lys38, Thr42, His128, and Leu129 of ECP are successively equivalent to Gln11, His12, Lys41, Thr45, His119, and Phe120 in RNase A.

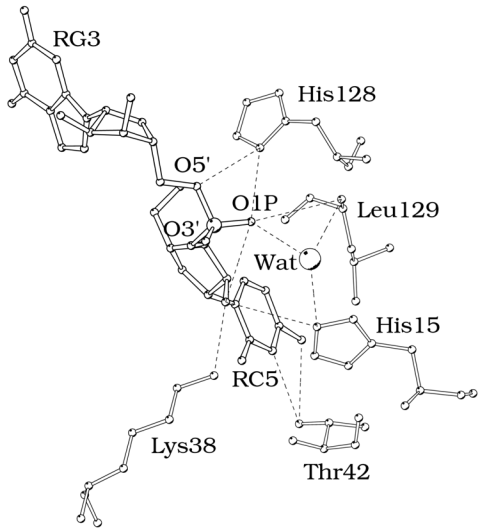

Figure 6: A schematic representation of the network of hydrogen bonds including the protein-ligand atoms and the water molecule obtained from the simulation of ECP-CpG complex. Very similar interactions are also obtained from the simulations of CpA and UpA bound complexes of ECP.

The active-site geometry is considered as a 'melting pot' on the basis of following observations emerging from the simulations of the dinucleotide bound complexes of ECP. (I) In spite of the fact that the protein-ligand complexes were generated independently for the three dinucleotides, namely CpG, CpA, and UpA, some of the protein-ligand interactions are consistently seen for a significant simulation time in all the three cases. (II) The residues and the atoms involved in the above interactions are those that were identified as necessary for the binding and the catalysis in earlier investigations. In our study, these residues form a network of connections leading to the simultaneous existence of the crucial interactions. (III) The geometry of the interacting residues at the active site is able to account for different mechanisms proposed earlier.

The relevant interactions and their significance to the mechanisms proposed earlier are briefly outlined here. The oppositely charged residues (*e.g*., negatively charged - OP1 of the phosphate group of the ligand, the positively charged amino group of Lys38) are part of the network. This has the advantage of facilitating the proton transfer (31) since the hydrogen bonding of the charged systems would be much stronger and shorter than a normal neutral hydrogen bond. This aspect was emphasized in the short-strong hydrogen model of Gerlt and Gassmann. The two crucial

histidines (His15 and His128), which are known to participate in the catalysis in the simultaneous two-proton-shift model (33), are also part of the present hydrogen bond network. In fact, both the histidines are simultaneously connected to O1P through a water molecule in the UpA complex (Figure 6). This water molecule is tightly held for most of the simulation time (Figure 4) in the CpA and CpG bound complexes as well. However, His128 is not a part of this network in these two complexes. The advantage of the participation of the water molecule in the active site is that in addition to occupying the cavity, it is involved in multiple hydrogen bonds imparting extra stability. This can lead to the formation of the crucial connections and help in the relay process of proton transfer. It should be noted that this water molecule also acquires a strong hydrogen bonding capability, since it is bonded to the negatively charged oxygen atom (O1P) of the phosphate moiety. It is likely that this water molecule, in addition to stabilizing the complex, might directly be involved in the hydrolysis itself upon forming a hydrogen bond with His128 (as has been shown possible in UpA complex). Furthermore, the O2′ atom of the ribose is known to be vital (21) in the formation of the cyclic phosphate intermediate structure during the cleavage of the phospho-diester bond. The hydrogen atom attached to the O2′ atom is proposed to be transferred to His15 (21). In our simulations we see intermittent direct hydrogen bond between the O2′ atom and His15(NE2) as well as a constant interaction through a water bridge. The intra-ligand proton transfer mechanism (33) speculates that the O2′ oxygen is involved in an intra-ligand proton transfer to the phosphorous atom of the phosphate group and also to the O3′ atom of the same ribose (44, 48). Our simulations indicate that the O2′ atom is hydrogen bonded with O3′ atom for sometime in all the three ligand bound complexes (Table V). Furthermore, the phosphorous atom of the phosphate moiety was also found to be within 3.6 Å (3.55 ± 0.3 Å) from the O2′ atom during the simulations. However, we note that the hydrogen bond of the O2′ atom with the phosphate oxygen (OP1) is present for a significant amount of simulation time. Thus, the active-site geometry, which is observed during the simulations, points to the fact that a complex network of interactions takes place during the catalysis and the reduction in the activation barrier is brought about by a multi-coordinated, concerted process. Such an active-site geometry, which is like a ‘melting-pot’, facilitates the simultaneous exchange of hydrogen bond-covalent character of several interactions because of a complex network of connections involving charged groups. The exact sequence of events and the strengths of interactions (a generous criterion of 3.5 Å is used to identify hydrogen bonds in the present simulations) however needs to be probed by high-level *ab initio* quantum chemical methods on the lines followed for the elucidation of catalytic mechanisms of other proteins (49, 50).

Conclusions

Eosinophil cationic protein (ECP) is a member of the Ribonuclease-A family. It performs the RNA hydrolysis along with a number of other important biological functions. Unlike in the case of RNase A, the availability of the ligand-bound structures of ECP was limited only for the ligand 2′-5′ ADP. In the present study, (a) the dinucleotide ligands are docked into the active-site of ECP and, (b) the dynamical properties of the bound and native structures of ECP are compared and (c) a consistent protein-ligand water interaction at the active-site of ECP is obtained by extensive molecular dynamics simulations.

The dinucleotide (CpG, CpA and UpA) bound structures of ECP were generated by considering the flexibility in the geometries of both the protein and the ligand. The flexible protein geometries were generated by 5 ns MD simulations on native ECP.

The important modes of the native and the ligand-bound structures were captured by the essential dynamics calculations. It is shown that the behavior of the top modes of the ligand-bound structures is quite different from that of the native protein, while they are very much similar to each other amongst the ligand-bound structures.

The ligands make most of the contacts essential for the binding of the pyrimidine base at the B1 subsite. The purine base at the B2 subsite is more flexible, a feature which is consistent with the observation on the ligand-bound structures of RNase A.

Water molecules, that form a stable network, connect several of the protein and the ligand atoms. Interestingly these networks found in the three ligand bound simulations connect the same residues in all the three simulations. This emphasizes the inherent property of proteins to retain water molecules at specific sites. More importantly, the active-site networks are reproduced in all the three ligand-bound structures and show some differences in interactions at this location from the native ECP.

A complex network of hydrogen bonds involving the protein-ligand and a water molecule at the active site persists during the dynamics timescale. We have referred to such an active-site geometry as the 'melting-pot'. The complex network involving the important ligand atoms like O2′ of ribose, the phosphate oxygen, the catalytically important protein residues such as His15, His128, and Lys38, a water molecule is ideally suited for changes in interactions, which take place during catalysis. The participation of a water molecule in the active site network facilitates the inter-linking of crucial atoms by providing scope for a relay of protons among them. While the resultant active site geometry accommodates many of the previously proposed mechanisms for RNA catalysis by Ribonuclease A, the complex protein-ligand network including water molecules obtained from the simulations calls for a re-evaluation of the existing mechanisms.

Acknowledgements

Partial support for this project was received from the Department of Science and Technology (DST), India [No SP/50/D-108/98], and from the Department of Biotechnology (DBT), India, through the Computational Genomics Initiative grant. Computational facility from the Super Computer Education and Research (SERC), Indian Institute of Science is acknowledged. One of us (B. S. S.) also thanks CSIR (India) for the fellowship.

References and Footnotes

1. M. Garcia-Viloca, J. Gao, M. Karplus, and D. G. Truhlar. *Science 303*, 186-195 (2004).
2. M. S. Madhusudhan and S. Vishveshwara. *Proteins 42*, 125-135 (2001).
3. K. Seshadri, V. S. Rao, and S. Vishveshwara. *Biophys. J. 69*, 2185-2194 (1995).
4. M. S. Madhusudhan and S. Vishveshwara. *Biopolymers 49*, 131-144 (1999).
5. B. S. Sanjeev and S. Vishveshwara. *Eur. Phys. J-D 20*, 601-608 (2002).
6. S. Vishveshwara, M. S. Madhusudhan, and J. V. Maizel, Jr. *Biophys. Chem. 89*, 105-117 (2001).
7. B. S. Sanjeev and S. Vishveshwara. *Proteins 55*, 915-923 (2004).
8. E. Boix. In *Methods in Enzymology*, Chapter 18, pp. 287-304, Ed., Nicholson, A. W. New York: Academic Press (2001).
9. J. B. Domachowske, K. D. Dyer, A. G. Adams, T. L. Leto, and H. F. Rosenberg. *Nucleic. Acids. Res. 26*, 3358-3363 (1998).
10. H. F. Rosenberg. *J. Biol. Chem. 270*, 7876-7881 (1995).
11. G. Mallorqui-Fernandez, J. Pous, R. Peracaula, J. Aymami, T. Maeda, H. Tada, H. Yamada, M. Seno, R. de Llorens, F. X. Gomis-Ruth, and M. Coll. *J. Mol. Biol. 300*, 1297-1307 (2000).
12. C. G. Mohan, E. Boix, H. R. Evans, Z. Nikolovski, M. V. Nogues, C. M. Cuchillo, and K. R. Acharya. *Biochemistry 41*, 12100-12106 (2002).
13. S. Sorrentino and M. Libonati. *FEBS Lett. 404*, 1-5 (1997).
14. M. S. Madhusudhan, B. S. Sanjeev, and S. Vishveshwara. *Proteins 45*, 30-39 (2001).
15. G. E. Cohen. *J. Appl. Crys. 30*, 1160-1161 (1997).
16. E. A. Merritt and D. J. Bacon. *Methods Enz. 277*, 505-524 (1997).
17. D. A. Case, *et al*. AMBER7, University of California, San Francisco (1997).
18. T. E. Cheatham, 3rd, P. Cieplak, and P. A. Kollman. *J. Biomol. Struct. Dyn. 16*, 845-862 (1999).
19. W. L. Jorgensen, J. Chandrasekhar, J. Madura, and M. L. Klein. *J. Chem. Phys. 79*, 926-935 (1983).
20. T. A. Darden, D. M. York, and L. G. Pedersen. *J. Chem. Phys. 98*, 10089-10092 (1993).
21. R. T. Raines. *Chem. Rev. 98*, 1045-1066 (1998).
22. A. Amadei, A. B. Linssen, and H. J. Berendsen. *Proteins 17*, 412-425 (1993).
23. B. L. de Groot, D. M. van Aalten, A. Amadei, and H. J. Berendsen. *Biophys. J. 71*, 1707-1713 (1996).

24. V. L. Murthy, R. Srinivasan, and G. D. Rose. *J. Mol. Biol. 291*, 313-327 (1999).
25. D. G. Gorenstein, B. A. Luxon, and J. B. Findlay. *Biochem. Biophys. Acta. 475*, 184-190 (1977).
26. D. G. Gorenstein. *Chem Rev. 94*, 1315-1338 (1994).
27. L. J. Murray, W. B. Arendall 3rd, D. C. Richardson, and J. S. Richardson. *Proc. Natl. Acad. Sci. USA 100*, 13904-13909 (2003).
28. A. Wlodawer. In *Biological Macromolecules and Assemblies. Vol 2 – Structure of Bovine Pancreatic Ribonuclease by X-Ray and Neutron Diffraction*, Chapter 9, pp. 393, Eds. Junark, F. A., McPherson, A. New York: John Wiley and Co. (1985).
29. C. M. Cuchillo, M. Vilanova, and V. Nogues. In *Ribonucleases: Structures and Functions*, pp. 284-285. Eds., D'Alessio, Riordan, J. F. Acedemic, New York (1996).
30. S. Sarkhel and G. R. Desiraju. *Proteins 54*, 247-259 (2004).
31. R. Breslow and W. H. Chapman, Jr. *Proc. Natl. Acad. Sci. USA 93*, 10018-10021 (1996).
32. J. A. Gerlt and P. G. Gassman. *Biochemistry 32*, 11943-11952 (1993).
33. C. Lim and P. Tole. *J. Am. Chem. Soc., 114*, 7245-7252 (1992).
34. J. F. Riordan. In *Ribonucleases, Structures and Functions*, Chapter 14, pp. 446-489, Eds., D' Alessio, G. and Riordan, J. F. New York: Acedemic Press (1997).
35. S. Sorrentino and M. Gleich. *FEBS Lett. 288*, 23-26 (1991).
36. M. R. Snyder and G. J. Gleich. In *Ribonucleases, Structures and Functions*, Chapter 13, 426-444. Eds., D' Alessio, G. and Riordan, J. F. New York: Acedemic Press (1997).
37. E. Boix, Z. Nikolovski, G. P. Moiseyev, H. F. Rosenberg, C. M. Cuchillo, and M. V. Nogues. *J. Biol. Chem. 274*, 15605-15614 (1999).
38. F. M. Richards and H. W. Wyckoff. In *The Enzymes, 3rd Ed., Vol. 4*, pp. 747-806. Ed., Boyer, P. D. Acedemic, New York (1971).
39. X. Pares, M. V. Nogues, R. de Llorens, and C. M. Cuchillo. *Eur. J. Biochem. 105*, 571-579 (1980).
40. G. L. Gilliland. In *Ribonucleases, Structures and Functions*, Chapter 10, pp. 306-341. Eds., D' Alessio, G. and Riordan, J. F. New York: Acedemic Press (1997).
41. D. D. Leonidas, R. Shapiro, S. C. Allen, G. V. Subbarao, K. Veluraja, and K. R. Acharya. *J. Mol. Biol. 285*, 1209-1233 (1999).
42. P. Blackburn and S. Moore. In *The Enzymes, 3rd Ed., Vol. 15*, pp. 317-433. Ed., Boyer, P. D. Academic, New York (1982).
43. R. L. Campbell and G. A. Petsko. *Biochemistry 26*, 8579-8584 (1987).
44. B. Wladkowski, M. Krauss, and W. Stevens. *J. Am. Chem. Soc. 117*, 10537-10545 (1995).
45. A. Dejaegere and M. Karplus. *J. Am. Chem. Soc. 115*, 5316-5317 (1993).
46. A. Dejaegere, X. Liang, and M. J. Karplus. *Chem. Soc. Faraday. Trans. 90*, 1763-1770 (1994).
47. A. Peeters and C. van Alsenoy. *Biopolymers 50*, 697-704 (1999).
48. P. Auffinger and E. Westhof. *J. Mol. Biol. 274*, 54-63 (1997).
49. M. A. Collins and L. Radom. *J. Chem. Phys. 118*, 6222-6229 (2003).
50. D. M. Smith, B. T. Golding, and L. Radom. *J. Am. Chem. Soc. 123*, 1664-1675 (2001).

Date Received: Needed

Communicated by the Editor Ramaswamy H Sarma